

Sensitivity of Global Modeling Initiative CTM predictions of Antarctic ozone recovery to GCM and DAS generated meteorological fields

David B. Considine
NASA Langley Research Center, Hampton, Virginia

Peter S. Connell, Daniel J. Bergmann, and Douglas A. Rotman
Lawrence Livermore National Laboratory

Susan E. Strahan
University of Maryland, Baltimore County, Baltimore, Maryland

Abstract. We use the Global Modeling Initiative chemistry and transport model to simulate the evolution of stratospheric ozone between 1995 and 2030, using boundary conditions consistent with the recent World Meteorological Organization ozone assessment. We compare the Antarctic ozone recovery predictions of two simulations, one driven by an annually repeated year of meteorological data from a general circulation model (GCM), the other using a year of output from a data assimilation system (DAS), to examine the sensitivity of Antarctic ozone recovery predictions to the characteristic dynamical differences between GCM and DAS – generated meteorological data. Although the age of air in the Antarctic lower stratosphere differs by a factor of 2 between the simulations, we find little sensitivity of the 1995-2030 Antarctic ozone recovery between 350 K and 650 K to the differing meteorological fields, particularly when the recovery is specified in mixing ratio units. Percent changes are smaller in the DAS-driven simulation compared to the GCM-driven simulation due to a surplus of Antarctic ozone in the DAS-driven simulation which is not consistent with observations. The peak ozone change between 1995 and 2030 in both simulations is ~20% lower than photochemical expectations, indicating that changes in ozone transport due to changing ozone gradients at 450 K between 1995 and 2030 constitute a small negative feedback. Total winter/spring ozone loss during the base year (1995) of both simulations and the rate of ozone loss during August and September is somewhat weaker than observed. This appears to be due to underestimates of Antarctic Cl_y at the 450 K potential temperature level.

1. Introduction

Observations over the last decade indicate that the burden of organic chlorine and bromine – containing compounds in the troposphere peaked during the mid 1990's and are now declining [WMO, 2003]. Stratospheric inorganic chlorine concentrations have leveled off, and may also soon be observed to be declining [*Rinsland et al.*, 2003; *Waugh et al.*, 2001]. Stratospheric chlorine and bromine concentrations are expected to decline over the next century provided that the halocarbon emission controls established by the Montreal Protocol and associated international agreements are followed [WMO, 2003].

Stratospheric ozone concentrations are expected to respond to these chlorine decreases due to the important role of halogens in ozone photochemistry [*Solomon*, 1999], and there is now some evidence pointing to a slowdown of the decreasing ozone trend in the upper stratosphere [*Newchurch et al.*, 2003]. The potential response of Antarctic ozone is interesting because of its high sensitivity to elevated halogen levels. In addition to changes in halogen loading, there are other factors which may influence Antarctic ozone such as changes in stratospheric temperature and dynamics due to the buildup of greenhouse gases, the chemical effects of continuing increases in methane (CH_4), nitrous oxide (N_2O), and water vapor, and changing stratospheric sulfate aerosol loading.

Accounting for the effects of these various factors challenges the scientific community interested in predicting the response of polar stratospheric ozone to future decreases in stratospheric chlorine/bromine loading. Much of the recent interest has focused on including dynamical and thermal responses to increased greenhouse gas concentrations, sparked by predictions of a very long delay in Arctic ozone recovery [*Shindell et al.*, 1998]. An intercomparison of several coupled chemistry/climate model predictions of both Arctic and

Antarctic ozone recovery was discussed in WMO [2003], and the intercomparison was also published in a peer reviewed journal article [*Austin et al.*, 2003].

Despite the interest in chemistry/climate feedbacks, there are other sources of uncertainty in model predictions of ozone recovery that deserve attention. For instance, the basic representation of stratospheric transport processes (polar and tropical transport barriers, residual circulation, etc.) might be important. However, we currently lack a quantitative understanding of the degree of uncertainty in recovery predictions caused by the uncertainties in modeling atmospheric transport. The goal of this paper is to improve our understanding of this relationship without the added complication of dynamical responses to global change.

Chemistry and transport models (CTMs) of the stratosphere do not generate their own dynamical fields. Instead they rely on externally-supplied meteorological data sets (temperatures, winds, etc.) to drive the CTM chemistry and transport modules. The meteorological data sets can be generated either by a free-running general circulation model (GCM) or a data assimilation system (DAS) (A DAS optimally combines observational information with GCM output to produce ostensibly more realistic meteorological data than is possible with a free-running GCM [*Coy and Swinbank*, 1997]). GCM and DAS meteorological data sets have characteristic differences, which will be discussed below. These differences allow us to test the response of a model ozone recovery prediction to a systematic and quantifiable change in model transport properties.

In this paper we intercompare two different simulations of Antarctic ozone recovery made with the Global Modeling Initiative (GMI) 3D Chemistry and Transport model [*Rotman et al.*, 2001]. The only difference between the two simulations is the meteorological data driving model transport. One is driven by a single year of output of a free-running GCM, repeated

annually for the duration of the simulation. The other uses a year of meteorological output generated by a DAS. All other aspects of the model including even the model advection algorithm and number and location of vertical levels, remain the same. Comparing simulations driven by these two meteorological data sets tests the sensitivity of Antarctic ozone recovery predictions to the characteristic differences between GCM-derived and DAS-derived meteorological data sets.

In section 2 we briefly describe the GMI model. In section 3 we outline the model experiments. In section 4 we show and interpret the results of the simulations. We provide a summary and conclusions in section 5.

2. Model Description

The GMI 3D CTM was first described by *Rotman et al.* [2001]. Application of the model to the potential impacts of stratospheric aircraft emissions is presented in *Kinnison et al.* [2001]. The model was used to investigate the effects of stratospheric aircraft emissions on the occurrence of polar stratospheric clouds (PSCs) in *Considine et al.* [2000].

The CTM as formulated for this study has a horizontal resolution of 5° longitude by 4° latitude, with 28 vertical levels. The interface between sigma (terrain-following) and constant pressure horizontal surfaces occurs at 247.46 hPa. The model extends up to .43 hPa, about the top of the stratosphere. The model uses externally-supplied meteorological data (surface pressures, horizontal winds, and temperature distributions) to drive the CTM. Model constituents are advected using the *Lin and Rood* [1997] advection scheme.

The CTM includes a full description of stratospheric chemistry including heterogeneous reactions on polar stratospheric clouds (PSCs). The photochemical scheme has been upgraded from *Rotman et al.* [2001] with improvements described in *Douglass et al.*, “Radicals and

reservoirs in the GMI chemistry and transport model: Comparison to measurements,” submitted to Journal of Geophysical Research, 2003 (hereafter referred to as Douglass2003). The chemical mechanism contains 56 species including the chlorine and bromine radical species which dominate polar ozone destruction during late winter and spring after activation by PSCs. Stratospheric water vapor distributions are based on observations made by the Microwave Limb Sounder (MLS) instrument on board the Upper Atmosphere Research Satellite (UARS) as described in *Rotman et al.* [2001]. The chemical mechanism is solved using the SMVGEAR II technique [*Jacobson, 1995; Jacobson and Turco, 1994*]. Two of the model transported species account for water vapor from the decay of stratospheric methane and dehydration due to nucleation of Type 2 (water ice) PSCs.

The PSC parameterization settings were changed from that described in *Considine et al.* [2000]; here, Type 1 PSCs were assumed to have a nitric acid trihydrate (NAT) composition with a number density of 0.1 cm^{-3} instead of supercooled ternary sulfate (STS) aerosols with a number density of 10 cm^{-3} . This choice results from a desire to better represent the PSC characteristics of the Arctic, where recent observations by *Fahey et al.* [2001] show extensive NAT particle formation and denitrification, and the recent study of *Considine et al.* [2003], which showed that STS aerosols are ineffective denitrifiers of the Arctic polar vortex due to their small size. The WMO 2002 background sulfate aerosol distribution is also included, which catalyzes heterogeneous reactions with the same temperature dependence as STS aerosols. Thus the only Type 1b (liquid) PSC processes which are neglected in this parameterization are the swelling of the PSCs at low temperatures due to HNO_3 uptake, and their sedimentation.

The current study utilized two sets of meteorological information (horizontal winds, surface pressures, and temperature distributions) to drive the CTM. These data sets were created

by the Goddard Space Flight Center Data Assimilation Office. The first was generated from a 50-year run of the “Finite Volume” General Circulation Model (FVGCM), a GCM jointly developed by NASA and the National Center for Atmospheric Research (NCAR). This GCM combines the physical parameterizations of the NCAR CCM3 GCM [Kiehl *et al.*, 1998] with the Lin and Rood [1997] advection scheme (See http://polar.gsfc.nasa.gov/sci_research/fvdas/index.php) for more details. The second set of meteorological data was generated by a recent version of the Goddard Earth Observing System Data Assimilation System (GEOS - DAS) [Schubert *et al.*, 1993], which uses the FVGCM to provide forecasts for the DAS. Schoeberl *et al.* [2003] provide a useful comparison of FVGCM and FVDAS characteristics. The FVGCM and FVDAS data sets have a resolution of 2.5° longitude by 2° latitude, with 55 vertical levels extending to 0.01 hPa. The FVGCM run was constrained with climatological sea surface temperatures, so year-to-year differences in this run are due to internal interannual variability. One year of meteorological data was selected from this simulation for use in the GMI CTM. The particular year was chosen on the basis of its relatively cold Arctic winter, for reasons unrelated to the work presented in this paper. The year of FVDAS data used in this study corresponds to July 1, 1999 through June 30, 2000.

Both sets of meteorological data were mapped to the same hybrid sigma-pressure coordinate system mentioned above (5° longitude by 4° latitude by 28 levels) for this study, using a divergence-preserving methodology [Rotman *et al.*, 2001]. The characteristics of these two mapped data sets and their ability to reproduce observed constituent distributions have been extensively evaluated by Strahan and Douglass [2004]. This study found that the GCM-derived meteorological data has a more realistic residual circulation and more credible tracer transport characteristics than does the DAS-derived data set.

3. Experiment Description

The two simulations using the GCM and DAS meteorological data sets will be referred to as the GMI_GCM and GMI_DAS simulations, respectively, for the remainder of this paper. The source gas boundary conditions used for the two simulations correspond to the MA2 scenario specified in Table 4B-1 of the WMO 2002 ozone assessment [WMO 2003]. The simulations were initialized similarly and spun up for five years at 1995 source gas boundary conditions. The simulations were then integrated forward in time for 36 years, through the year 2030. It is important to remember that the meteorological fields used are for a single year which is recycled for each year of the simulation, so this study does not address the possible effects of dynamical and thermal changes on constituent evolution. Halocarbon surface mixing ratios were specified from Table 4B-2 of the WMO assessment report. CH₄ and N₂O mixing ratios were specified as scenario A2 of the International Panel on Climate Change 2001 report, also listed in Table 4B-3 of the WMO assessment.

The background sulfate aerosol distribution was specified using the WMO 2002 assessment aerosol data set. The aerosols followed observed values from 1995 to 1999. Between 2000 and 2030, the aerosol distribution for 1997 was repeated annually.

For both simulations the year of data used extends from July 1, through June 30. Thus on each year of the 36 year simulation there is a discontinuity between June 30 and July 1. This means that each Antarctic winter/spring season is actually preceded by the summer/fall season which followed the winter/spring season in the meteorological data, instead of the preceding summer/fall season. The influence of this change on the Antarctic winter/spring will depend on the extent of the differences between the two summer/fall seasons and the amount of influence the Antarctic summer/fall season has on a subsequent winter/spring. Because interannual

variability in the Antarctic lower stratosphere is relatively small and the goal of this paper is to compare simulations driven by two statistically distinct meteorological data sets (that is, separated by differences which are larger than interannual variability), we feel that the presence of the discontinuity will not affect the conclusions of this paper.

The model diagnostics used in the following analysis consist of species mixing ratios written out at 0Z every 3 days during 1995 and during 2030. The analysis also uses three-day average reaction rates, again written out at 0Z every 3 days.

4. Results

4.1 Dynamical Differences

In this section we seek to quantify the dynamical differences between the two meteorological data sets in terms that are meaningful for stratospheric tracer transport and composition. One important measure of stratospheric transport characteristics is the mean age of stratospheric air, and its distribution in latitude and altitude. The mean age of the air at a particular latitude and altitude can be thought of as the average time for a parcel of air to travel from the ground to that location. The mean age is therefore an integral property of stratospheric transport; that is, its value at any location characterizes the influence at that point of the transport characteristics of the entire stratosphere [Hall and Plumb, 1994; Waugh and Hall, 2002]. It has been used previously as a measure of model transport properties in a large model intercomparison exercise [Hall *et al.*, 1999].

Figure 1 shows the vertical and meridional distribution of the mean age of air calculated from simulations using the GCM (Figure 1a) and DAS (Figure 1b) wind fields described above. Figure 1c shows the difference between the two age distributions, and Figure 1d compares the simulated mean ages with values inferred from NASA ER-2 aircraft observations of CO₂

[Boering *et al.*, 1996]. Figure 1a shows that the GCM meteorological data produces a mean age of $\sim 5.5 - 6$ years in the upper stratosphere. The DAS-derived upper stratospheric mean age shown in Figure 1b is ~ 2 years younger. In the upper stratosphere the GCM-derived mean age is in much better agreement with observationally-derived estimates. Figure 1d shows that this is also the case in the lower stratosphere [Hall *et al.*, 1999; Waugh *et al.*, 2001]. The mean age differences shown in Figure 1 are typical of GCM-based and DAS-based circulations. Residual circulations inferred from analyzed meteorological data are generally too vigorous, producing young stratospheric air. [Considine *et al.*, 2003; Schoeberl *et al.*, 2003; Weaver *et al.*, 1993].

Distributions of long-lived tracers such as N_2O and CH_4 can also provide information about transport differences between the GMI_GCM and GMI_DAS simulations. Figures 2a and 2b show equivalent-latitude averaged N_2O in September on the 650 K and 450 K potential temperature surfaces, respectively, as a function of equivalent latitude, from the GMI_GCM and GMI_DAS simulations. The figure also shows equivalent latitude averaged N_2O distributions derived from Cryogen Limb Array Etalon Spectrometer (CLAES) satellite observations made during September, 1992, at 650 K and 450 K [Roche *et al.*, 1996]. At 450 K, Airborne Tunable Laser Absorption Spectrometer (ATLAS) observations made during the September, 1987 flights of the Airborne Antarctic Ozone Experiment (AAOE) and the October, 1994 flights of the Airborne Southern Hemisphere Ozone Experiment (ASHOE) are included as well [Loewenstein *et al.*, 1989; Loewenstein *et al.*, 1990].

The simulated and observed N_2O distributions all exhibit the familiar “roller coaster” pattern caused by lower stratospheric dynamical processes at both 450 K and 650 K. At 650 K, the gradient separating the tropics from the midlatitudes is substantially weaker in the GMI_DAS simulation than in either the CLAES observations or the GMI_GCM simulation. The gradients

separating the midlatitudes from the polar vortex are similar in both simulations at 650 K and are weaker than observed. The weaker gradients at the vortex edge indicate that the meridional mixing between the vortex and midlatitudes is too strong relative to the descent rate of air within the vortex in both simulations.

At 450 K the subtropical N₂O gradients separating the tropics from the midlatitudes are similar in both simulations and are weaker than are observed. At high latitudes the GMI_GCM N₂O distributions agree better with observations than the GMI_DAS simulation, suggesting a somewhat more isolated and realistic representation of the polar vortex.

Overall, the GMI_GCM simulation more convincingly reproduces observed N₂O distributions. The differences between the simulated N₂O distributions are consistent with the younger age of high-latitude air in the GMI_DAS simulation and further illustrate a characteristic problem with CTM simulations driven by DAS-generated wind fields. Further evaluation of the different effects of the transport fields on stratospheric tracer distributions is provided in *Strahan and Douglass* [2004].

Another potentially important difference to consider is the occurrence of temperatures low enough to provoke formation of PSCs. The occurrence of these low temperatures in the two simulations is shown in Figure 3. Figure 3a shows the size of the Southern Hemisphere extratropical region below 195 K (the approximate temperature below which PSCs can form) as a function of day of year and potential temperature in the GMI_GCM simulation. This “cold pool” area is expressed as a fraction of the total global area. Figure 3b shows the same plot for the GMI_DAS simulation. Figures 3a and 3b demonstrate a qualitatively similar morphology, with the coldest temperatures (the largest cold pool areas) occurring earlier in the year at higher potential temperatures. Figure 3c shows the percent difference between the GMI_GCM and

GMI_DAS cold pool areas wherever the GMI_DAS cold pool area is larger than 1% of the total area of the globe. Figure 3c shows that the GMI_GCM cold pool area is smaller than GMI_DAS by ~30% in late fall at potential temperatures of ~550-600K. Also, the GMI_DAS cold pool area is substantially larger than GMI_GCM after day 280 between ~350-500K. However, the GMI_GCM cold pool exceeds GMI_DAS during the critical months of August and September by up to 10% at ~600K increasing to ~50% at lower potential temperatures near ~350K. At ER-2 aircraft flight altitudes the differences in cold pool areas between the two simulations infrequently exceed $\pm 10\%$.

4.2 1995-2030 Changes in Ozone

In Section 4.1 we established that the dynamical differences between the FVGCM and FVDAS meteorological data sets produce large differences in the mean age of air in the Antarctic lower stratosphere. Long-lived tracer distributions were also different, though the high-latitude differences appear to be smaller than those seen in the subtropics. We also noted more modest thermal differences between the two simulations. These differences may influence the manner in which Antarctic ozone responds to decreases in halocarbon emissions at the surface. In this section we examine the changes in Antarctic ozone between 1995 and 2030 to establish the extent to which the meteorological differences influence ozone response.

Figure 4 shows the change in Antarctic ozone mixing ratios in response to source gas forcing between 1995 and 2030 as a function of day of year and potential temperature in the GMI_GCM (Figure 4a) and GMI_DAS (Figure 4b) simulations. The figures show an average over equivalent latitudes “poleward” of -65° equivalent latitude. We will use such averages throughout this paper to provide a measure of average constituent behavior in the Antarctic. Figures 4a and 4b show similar changes in Antarctic ozone in these two simulations. In the

GMI_GCM simulation, the peak ozone increase of 0.76 ppmv occurs at ~500 K on Julian day 278, in early October. At 450 K, the peak occurs 3 days later and reaches 0.7 ppmv. In the GMI_DAS simulation, the peak ozone increase of 0.70 ppmv also occurs at 500 K on day 278. At 450 K, the peak increase is 0.66 ppmv. Thus, the GMI_GCM peak is ~6% larger than in the GMI_DAS at 450 K and ~8.5% larger at 500 K. The Antarctic ozone recovery predictions display little sensitivity to the meteorological differences which lead to the age differences shown in Figure 1. Larger differences between the GMI_GCM and GMI_DAS simulations are shown in Figures 5a and 5b, which show the percentage differences in Antarctic ozone between 1995 and 2030 in the GMI_GCM (5a) and GMI_DAS (5b) simulations. In contrast to Figure 4, the peak 1995-2030 change in Antarctic ozone of ~40% occurs at 450 K in the GMI_GCM simulation, while there is a smaller increase of ~28% in the GMI_DAS simulation at 400 K. Peak percent changes occur at about the same day of the year, but occur ~50 K and ~100 K lower in potential temperature than the locations of the peak mixing ratio differences in the GMI_GCM and GMI_DAS simulations, respectively.

The relative GMI_GCM peak shown in Figure 5a is ~43% larger than the GMI_DAS peak shown in Figure 5b even though the peak 1995-2030 mixing ratio differences are similar. This is due to different simulations of the base year (1995). Figure 6 compares Antarctic ozone mixing ratios from the two simulations for the base year on the 450 K (Figure 6a), 550 K (Figure 6b), and 650 K (Figure 6c) potential surfaces. Both simulations have the same general morphology, with peak ozone occurring in the winter and minima during the late spring. However, there is generally more Antarctic ozone in the GMI_DAS simulation. Figure 6a shows that there is up to ~1.0 ppmv more ozone in the GMI_DAS simulation at 450 K than in the

GMI_GCM simulation. The higher ozone mixing ratios in the GMI_DAS simulation produce the smaller relative 1995-2030 differences shown in Figure 5b.

Also included in the figure are observed values from 1992 (red crosses), 1993 (blue crosses), and 1994 (green crosses) version 5 MLS measurements [*Froidevaux et al.*, 1996; *Livesey et al.*, 2003], and 1992 version 9 CLAES observations [*Bailey et al.*, 1996]. The GMI_GCM simulation agrees better than the GMI_DAS simulation with the MLS ozone measurements at 450 K after day 180 and throughout the year at 550 K. At 650 K, both model simulations exhibit an annual cycle which is more pronounced than seen in the observations. Note that the MLS observations at 450 K suffer from an instrumental artifact which results in higher ozone mixing ratios during the middle of a yaw cycle than at the beginning or end. This artifact is particularly noticeable during the winter yaw cycle of 1993 in Figure 6a. The cause of the artifact is not well understood [*Froidevaux et al.*, 1996], but the few tenths of a part per million variation does not seriously affect this qualitative comparison. The artifact is known to be smaller in version 5 retrievals than previously [*William G. Read, private communication*, 2003]. There are significant differences between the 1992 MLS and CLAES observations during the fall and winter yaw cycles. The model simulations are in closer agreement with the MLS observations during these times. At other times of year the CLAES and MLS observations agree well with each other.

This section shows that the 1995-2030 increase in ozone is not very sensitive to the dynamical differences between the two simulations, although the base year simulation is more sensitive. This is interesting because percent differences, which are obviously affected by the base year simulation, are typically compared in assessment exercises rather than mixing ratio differences. Such an approach may introduce substantial intermodel variability into an

assessment exercise as a consequence, even in cases where the various model responses are similar in terms of mixing ratio.

We compare in the next section the evolution of ozone over the course of the 1995 winter/spring season, both to understand the manner in which base year ozone concentrations evolve and are determined by springtime chemical and dynamical influences, and as a springboard for examining the sensitivity of the 1995-2030 increase in ozone to the dynamical differences between the two simulations,

4.3 Evolution of ozone in 1995

We choose to examine in detail the evolution of Antarctic ozone from winter through spring in the base year of the simulations at 450 K potential temperature level, because peak 1995-2030 ozone changes in both simulations occur within 50 K of this surface, with the changes expressed either as a mixing ratio or a percentage difference. We also use July 1 as a reference point to compare specifically the springtime ozone evolution. The solid line in Figure 7a shows the change in Antarctic ozone (i.e., the loss of ozone) after July 1 in the GMI_GCM simulation at 450 K. Two other lines are also shown on this plot. The dashed line shows the integrated chemical loss of ozone after July 1, calculated from model chemical rate diagnostic output. The dash-dot line shows the difference between the actual loss of ozone and the integrated chemical loss of ozone, which indicates the influence of transport. The red, blue, and green crosses in Figure 7a show changes in Antarctic ozone mixing ratios after July 1 calculated from ozone observations made in 1992, 1993, and 1994, respectively, by the Microwave Limb Sounder (MLS) instrument.

Figure 7a shows that over the course of the winter and spring seasons the GMI_GCM simulation has a maximum loss of ozone of ~1.9 ppmv. The solid line showing the actual ozone

loss in the model tracks very close to the dashed line showing integrated chemical loss through ~day 280 (early October). This indicates that at this potential temperature the evolution of ozone is dominated by chemical loss and ozone transport plays a minor role - through day 280, Figure 7a suggests that transport has reduced ozone loss by ~9%. Note however that this fact does not mean that transport is unimportant – just that changes in ozone due to the transport of ozone itself are small compared to changes in ozone due to in-situ photochemistry. The in-situ photochemistry may be substantially influenced by transport, for instance of Cl_y . After day 280 net ozone loss (solid line) remains steady while the integrated chemical loss term continues to drop by about 0.5 ppmv through the end of the year. Ozone is thus being transported into the region during this time to balance the continuing chemical loss. The fact that ozone transport is small during the August/September time frame is consistent with the results of *Wu and Dessler* [2001], which compared ozone loss at 465 K observed by MLS with estimates of chemical loss based on MLS observations of ClO during August and September of 1992, 1993, and 1994.

Comparison of the simulated ozone in Figure 7a with the MLS observations shows that the ozone loss is about 20% lower than the average observed ozone loss during 1992, 1993, and 1994. Also, averaged over the UARS springtime yaw cycle, the simulated rate of change of ozone is ~30% smaller than is observed - ~28.5 ppbv/day compared to the observed ~41.4 ppbv/day (we average over the yaw cycle to remove the effects of the instrumental artifact discussed above).

Figure 7b shows the same comparison as in Figure 7a for the GMI_DAS simulation. The figure shows that there are strong similarities with the GMI_GCM results shown in Figure 7b. The maximum loss of ozone is ~2.2 ppmv at about day 330. Although transport causes an initial deviation from the chemical loss in late July (~day 200), simulated ozone loss is virtually

identical to the chemical loss by day 280, and approximately parallels the integrated chemical loss through about day 300 (late October). In contrast to the GMI_GCM results, during the last two months of the year, model ozone loss exceeds the integrated chemical loss, implying that transport acts to reduce ozone after about day 300 (Note that transport is acting to reduce Antarctic ozone concentrations from day 200 on, but the net effect of transport is near zero through day 300). Kinematic back-trajectory calculations of high equivalent latitude parcels initialized at 450 K indicate that this is due to transport of some air with smaller ozone mixing ratios to the 450 K level from below.

As above, the overall loss is somewhat low compared to observations. The ozone loss rate of ~26.1 ppbv/day during the August/September time period is also substantially weaker than observed and slightly weaker than in the GMI_GCM simulation. Interestingly, Figure 7b shows that ~4 ppbv/day of the loss rate during August/September is due to transport, or about 16%. Without the transport contribution, the chemical loss rate is ~23% smaller than the GMI_GCM loss rate. The total chemical loss is 1.9 ppmv, which is about 18% smaller than the chemical loss in the GMI_GCM simulation.

We next examine in more detail the photochemistry of the two simulations to determine the causes of these differences.

4.4 Photochemistry in 1995

The primary deficiency of the model calculations shown in Figure 7 is the weak ozone loss compared to the MLS observations in the August/September time frame, particularly in the GMI_DAS simulation. Virtually all of the ozone destruction (> 93%) at this time in the two simulations is caused by catalytic cycles involving Cl_y and Br_y radical species.

We refer to the sum of the radical ClO and its nighttime reservoir Cl₂O₂ as “active chlorine,” and denote it by the symbol Cl_x. Figure 8a shows high-latitude averaged Cl_x and Cl_y on the 450 K surface between days 100 and 350 from both simulations. The figure shows that Cl_y peaks in August in both simulations with values of ~2.3 ppbv for GMI_GCM and ~1.8 ppbv for GMI_DAS – ~22% less and consistent with the smaller total springtime chemical loss of ozone for the GMI_DAS simulation shown in section 4.3. The larger Cl_y mixing ratios in the GMI_GCM simulation result in larger Cl_x mixing ratios for this simulation as well. Figure 8b compares the ratio Cl_x / Cl_y in the two simulations. Peak Cl_x activation exceeds 85% in both simulations. The ratio is similar during August/September, dropping from ~80% to ~60% by mid-September. The similarity of the ratio indicates that the weaker GMI_DAS ozone loss during this time shown in Figure 7b is due to lower Cl_y at 450 K, rather than differences in chlorine activation.

Also shown in Figure 8a is an estimate of Cl_y derived from CLAES N₂O observations made during the Antarctic winter/spring of 1992 using the Cl_y/N₂O relationship derived in *Woodbridge et al.*, [1995]. During September (days ~244 – 273), the Cl_y in the GMI_GCM simulation agrees reasonably well with the observational estimates although observationally-inferred Cl_y is apparently increasing during this time while the simulated Cl_y is beginning to drop from a winter peak. The Cl_y in the GMI_DAS simulation is low by ~0.5 ppbv. The observational estimate suggests that Cl_y increases until December, which is contrary to the decreasing trend in both simulations. This late-year discrepancy has little impact on simulated ozone loss because the Cl_x/Cl_y ratio falls to very low values by this time due to the return of sunlight and warm temperatures to high latitudes. More detail on the evolution of high latitude

tracer concentrations during the Southern Hemisphere springtime is given in *Strahan and Douglass* [2004].

We can also estimate Cl_y from the lower stratospheric high latitude N_2O observations made during the AAOE and ASHOE expeditions which are shown in Figure 2. Figure 9 shows these observed estimates of Cl_y and simulated Cl_y at 450 K as a function of equivalent latitude. All three of the observational estimates exceed both the GMI_GCM and GMI_DAS simulations throughout the southern hemisphere. At midlatitudes both simulations are quite a bit lower than the observational estimates, likely due to the very weak meridional gradient across the subtropics. At high latitudes the GMI_GCM simulated Cl_y is ~15% low, while the GMI_DAS underestimate at high latitudes is ~30%.

Wu and Dessler [2001] estimate from MLS ClO observations vortex-averaged Cl_x mixing ratios of ~2 – 2.5 ppbv at 465 K during the late August/early September period in 1992, 1993, and 1994. Figure 8a shows that Cl_x in the GMI_GCM simulation is about 15% to 20% lower than this estimate, and Cl_x in the GMI_DAS simulation is about 30% to 35% low. These deficits are consistent with the Cl_y comparisons shown above and could account for the weak August/September loss rate seen in the GMI_GCM and GMI_DAS simulations.

Figures 8 and 9 show that the in-situ photochemistry which controls Antarctic lower stratospheric ozone loss is affected by the differences in atmospheric transport which lead to the age discrepancies shown in Figure 1. Some combination of higher meridional mixing and/or lower vertical descent of air at high latitudes in the GMI_DAS simulation results in lower Cl_y mixing ratios at 450 K than in the GMI_GCM simulation. The result is about 20% lower total chemical ozone loss and a correspondingly smaller chemical ozone loss rate during August/September. Similarly, both Cl_x and Cl_y in the GMI_GCM simulation appear to be about

20% lower than observed values. These differences are relatively modest considering that the age of lower stratospheric Antarctic air differs by about a factor of 2 in the two simulations.

4.5 Chemistry and transport contributions to 1995 – 2030 ozone change

In section 4.2 above we showed that the peak 1995-2030 increase in Antarctic ozone at 450 K in the GMI_GCM simulation is only ~6% larger than the peak increase in the GMI_DAS simulation, despite the substantial dynamical differences in the meteorological data driving the two simulations discussed in section 4.1. Section 4.3 showed that the meteorological differences cause ~20% differences between the GMI_GCM and GMI_DAS simulations in the springtime chemical ozone loss during the base year of the simulations. Because ozone loss in both simulations is chemically controlled during the winter/spring, this is due largely to the effects of transport on Cl_y (and by implication, Br_y). To try to determine why the peak 1995-2030 increases in the two simulations differ only by ~6% while springtime ozone loss for the base years differ by ~20%, we now examine the individual chemistry and transport contributions to the 1995-2030 ozone change.

Figure 10a shows the high latitude winter/spring ozone loss in the GMI_GCM and GMI_DAS simulations at 450 K for 1995 (solid lines), 2030 (dashed lines) and the difference between 1995 and 2030 (dashed-dot lines). The figure shows that while the winter/spring ozone losses in the GMI_GCM and GMI_DAS simulations differ in timing and magnitude, the 1995-2030 difference in ozone loss in each of these two simulations is very similar, consistent with the differences shown in Figure 4 above. Peak values of the difference are 0.56 ppmv on day 281 in the GMI_GCM simulation and 0.51 ppmv on day 275 in the GMI_DAS simulation. Thus, the GMI_GCM 1995-2030 peak “recovery” of Antarctic ozone is slightly less than 10% larger than the recovery in the GMI_DAS simulation.

Figure 10b shows the winter/spring chemical loss of ozone in 1995 (solid blue (GCM) and red (DAS) lines) and 2030 (dashed blue and red lines) in the two simulations, in addition to the 1995-2030 change in winter/spring chemical loss at 450 K for the simulations (dash-dot blue and red lines). On the days of the peak 1995-2030 change in ozone loss for the two model simulations shown in Figure 10a, the 1995-2030 change in chemical loss is 0.69 ppmv for the GMI_GCM simulation and 0.66 ppmv for the GMI_DAS simulation. When only the change in chemical loss is considered, the GCM-driven simulation is just 4.5% larger than the DAS-driven simulation.

At the same time, the blue and red solid lines in Figure 10b show that the 1995 chemical loss from July 1 through the day of peak recovery is ~2.1 ppmv in the GMI_GCM simulation and ~1.5 ppmv in the GMI_DAS simulation. So, even though the GCM-driven simulation has a chemical ozone loss that is ~38% larger than the DAS-driven simulation at this time, the change in the chemical ozone loss between 1995 and 2030 is only slightly larger (4.5%) than the DAS-driven simulation. This will be discussed further below.

Figure 10c shows the effects of transport on ozone loss in 1995 (solid lines) and 2030 (dashed lines) for the GMI_GCM (blue) and GMI_DAS (red) simulations. It also shows the 1995-2030 difference (dash-dot lines) for each of the simulations. The 1995-2030 differences are relatively similar between the two simulations, with the GMI_DAS transport contribution slightly more negative than GMI_GCM. Note that since the 1995-2030 change in ozone transport is due entirely to changes in ozone gradients in the Antarctic (the wind fields themselves are the same every year), a negative contribution from transport is expected due to weaker ozone gradients in 2030 compared to 1995. On the day of peak ozone recovery (Figure

10a), the effect of changes in transport is to reduce the recovery peak by ~19% in the GMI_GCM simulation and ~23% in the GMI_DAS simulation.

Figure 10 shows that the effect of changes in the role of ozone transport between 1995 and 2030 is to create a larger difference in the ozone recovery of these two simulations, rather than a smaller difference. In the absence of the transport effects, the difference between the two simulations would simply be that of the 1995-2030 changes in chemical ozone loss - ~4.5%. Ozone transport is therefore not obscuring a larger difference between the simulations in the response of Antarctic photochemistry to the 1995-2030 changes in source gas forcing. Figure 10 therefore eliminates one possible transport-related explanation for the similarity of the 1995-2030 ozone response in the two simulations.

Figures 7a and 7b show that the bulk of the springtime ozone loss in both simulations occurs between days 220 and 280. The decreases in Cl_x and Cl_y from 1995 to 2030 that occur during this time period will determine how ozone changes due to photochemistry between 1995 and 2030. Figure 11 shows these decreases in Cl_x and Cl_y from 1995 to 2030 for both the GMI_GCM and GMI_DAS simulations. Figure 11 shows that the 1995-2030 change in Cl_y in the GMI_DAS simulation is about 10% smaller than the corresponding change in the GMI_GCM simulation. This is about half of the amount by which 1995 Cl_y in the GMI_DAS simulation differs from the GMI_GCM simulation. Figure 11 also shows that the 1995-2030 change in Cl_x in the GMI_DAS simulation is about the same as corresponding change in the GMI_GCM simulation. This implies that in the GMI_DAS simulation the Cl_x/Cl_y ratio has decreased between 1995 and 2030, making the overall decline in Cl_x about the same as in the GMI_GCM simulation. Although it is not clear exactly why the Cl_x/Cl_y ratio decreases more in the GMI_DAS simulation than in the GMI_GCM simulation, its stronger decrease results in a

more similar 1995-2030 change in chemical ozone loss in the two simulations than the differences in the 1995-2030 change in Cl_y suggest.

5. Summary and Conclusions

We have used the GMI 3D CTM to simulate ozone recovery over the the 1995 – 2030 time period using two different representations of atmospheric transport processes. We have compared Antarctic ozone recovery predictions generated in these two simulations to evaluate the sensitivity of the recovery predictions to the characteristic differences between GCM and DAS meteorological data sets. Our simulations do not consider the potential effects of climate change on ozone recovery.

The simulation driven by the GCM meteorological fields realistically captures the age of air distribution of the stratosphere, while the age of stratospheric air in the DAS-driven simulation is up to 2.5 years younger than observed. The GCM-driven simulation also has a more realistic representation of long lived trace species, as demonstrated by the comparison of simulated and observed N_2O . Both simulations have similar cold pool regions in the polar southern hemisphere, a fact which makes the intercomparison of the simulations a more direct test of dynamical sensitivity than would otherwise be the case.

Despite the substantial age differences in the two simulations, the 1995-2030 response of ozone mixing ratios between 350 K and 650K at Antarctic latitudes to changes in trace gas forcing is very similar. This indicates that the meteorological differences between the simulations do not strongly influence the 1995-2030 ozone change. One cannot therefore argue that a DAS-generated meteorological data set, or any set which underestimates stratospheric age, is automatically inappropriate for making ozone recovery calculations. Differences between

long-lived tracers in the Antarctic lower stratosphere provide a better indicator of response to changes in source gas boundary conditions.

The percent change of Antarctic ozone to source gas forcing between 1995 and 2030 shows larger differences between the two meteorological data sets and is stronger in the simulation driven by GCM output due to lower Antarctic ozone concentrations in the base year of the simulation. The utility of relative ozone change as a measure of recovery therefore depends on how well the current year is simulated.

The lower ozone in the GMI_GCM simulation is in better agreement with observations. In the absence of other factors which could affect recovery, such as changes in stratospheric temperatures or water vapor, the recovery prediction of the GMI_GCM simulation would be more credible as a result.

Antarctic winter/spring ozone loss at 450 K in both simulations is driven primarily by photochemistry through the end of October, and ozone transport to or from the vortex at 450 K plays only a small and similar role during this time. This result is consistent with observed behavior. Total ozone loss in both simulations agrees reasonably well with observations in both simulations, but the rate of ozone loss during the August/September time period is weak. The weak loss appears to be explained by low Cl_x at high latitudes, which is due in large part to low Cl_y .

These results have implications for the types of model intercomparisons used in the WMO assessment reports. These assessments typically present model results in terms of percent rather than mixing ratio differences from some base year, for instance 1980 (see for example Figure 4-42 of WMO [2003]). If absolute differences were used instead the intermodel variability seen in such figures may be significantly reduced.

Acknowledgements: The authors would like to thank Anne R. Douglass (NASA Goddard Space Flight Center), Andrew E. Dessler (University of Maryland Earth System Science Interdisciplinary Center), and William G. Read (Jet Propulsion Laboratory) for helpful discussions. This research was funded by the NASA Atmospheric Chemistry, Modeling and Analysis Program (ACMAP). Participation of Lawrence Livermore National Laboratory authors occurred through the University of California under the auspices of the U.S. Department of Energy contract W-7405-ENG-48.

References

- WMO (World Meteorological Organization), Scientific assessment of ozone depletion: 2002, Global Ozone Research and Monitoring Project - Report No. 47, 498 pp., Geneva, 2003
- Austin, J., et al., Uncertainties and assessments of chemistry-climate models of the stratosphere, *Atmospheric Chemistry and Physics*, 3, 1-27, 2003.
- Bailey, P.L., et al., Comparison of cryogenic limb array etalon spectrometer (CLAES) ozone observations with correlative measurements, *Journal of Geophysical Research-Atmospheres*, 101 (D6), 9737-9756, 1996.
- Boering, K.A., S.C. Wofsy, B.C. Daube, H.R. Schneider, M. Loewenstein, and J.R. Podolske, Stratospheric mean ages and transport rates from observations of carbon dioxide and nitrous oxide, *Science*, 274 (5291), 1340-1343, 1996.
- Considine, D.B., A.R. Douglass, P.S. Connell, D.E. Kinnison, and D.A. Rotman, A polar stratospheric cloud parameterization for the global modeling initiative three-dimensional model and its response to stratospheric aircraft, *Journal of Geophysical Research-Atmospheres*, 105 (D3), 3955-3973, 2000.
- Considine, D.B., S.R. Kawa, M.R. Schoeberl, and A.R. Douglass, N₂O and NO_y observations in the 1999/2000 Arctic polar vortex: Implications for transport processes in a CTM, *Journal of Geophysical Research-Atmospheres*, 108 (D5), 4170, doi:10.1029/2002JD002525, 2003.
- Coy, L., and R. Swinbank, Characteristics of stratospheric winds and temperatures produced by data assimilation, *Journal of Geophysical Research-Atmospheres*, 102 (D22), 25763-25781, 1997.

- Fahey, D.W., et al., The detection of large HNO₃-containing particles in the winter arctic stratosphere, *Science*, 291 (5506), 1026-1031, 2001.
- Froidevaux, L., et al., Validation of UARS microwave limb sounder ozone measurement, *Journal of Geophysical Research-Atmospheres*, 101 (D6), 10017-10060, 1996.
- Hall, T.M., and R.A. Plumb, Age as a Diagnostic of Stratospheric Transport, *Journal of Geophysical Research-Atmospheres*, 99 (D1), 1059-1070, 1994.
- Hall, T.M., D.W. Waugh, K.A. Boering, and R.A. Plumb, Evaluation of transport in stratospheric models, *Journal of Geophysical Research-Atmospheres*, 104 (D15), 18815-18839, 1999.
- Jacobson, M.Z., Computation of Global Photochemistry with Smvgear-Ii, *Atmospheric Environment*, 29 (18), 2541-2546, 1995.
- Jacobson, M.Z., and R.P. Turco, Smvgear - a Sparse-Matrix, Vectorized Gear Code for Atmospheric Models, *Atmospheric Environment*, 28 (2), 273-284, 1994.
- Kiehl, J.T., J.J. Hack, G.B. Bonan, B.A. Boville, D.L. Williamson, and P.J. Rasch, The National Center for Atmospheric Research Community Climate Model: CCM3, *Journal of Climate*, 11 (6), 1131-1149, 1998.
- Kinnison, D.E., et al., The Global Modeling Initiative assessment model: Application to high-speed civil transport perturbation, *Journal of Geophysical Research-Atmospheres*, 106 (D2), 1693-1711, 2001.
- Lin, S.J., and R.B. Rood, An explicit flux-form semi-Lagrangian shallow-water model on the sphere, *Quarterly Journal of the Royal Meteorological Society*, 123 (544), 2477-2498, 1997.
- Livesey, N.J., W.G. Read, L. Froidevaux, J.W. Waters, M.L. Santee, H.C. Pumphrey, D.L. Wu, Z. Shippony, and R.F. Jarnot, The UARS microwave limb sounder version 5 data set:

- Theory, characterization, and validation, *Journal of Geophysical Research-Atmospheres*, 108 (D13), doi:10.1029/2002JD002273, 2003.
- Loewenstein, M., J.R. Podolske, K.R. Chan, and S.E. Strahan, Nitrous-Oxide as a Dynamical Tracer in the 1987 Airborne Antarctic Ozone Experiment, *Journal of Geophysical Research-Atmospheres*, 94 (D9), 11589-11598, 1989.
- Loewenstein, M., J.R. Podolske, and S.E. Strahan, Atlas Instrument Characterization - Accuracy of the Aase and Aaoe Nitrous-Oxide Data Sets, *Geophysical Research Letters*, 17 (4), 481-484, 1990.
- Newchurch, M.J., E.S. Yang, D.M. Cunnold, G.C. Reinsel, J.M. Zawodny, and J.M. Russell, Evidence for slowdown in stratospheric ozone loss: First stage of ozone recovery, *Journal of Geophysical Research-Atmospheres*, 108 (D16), 2003.
- Rinsland, C.P., et al., Long-term trends of inorganic chlorine from ground-based infrared solar spectra: Past increases and evidence for stabilization, *Journal of Geophysical Research-Atmospheres*, 108 (D8), 4252, doi:10.1029/2002JD003001, 2003.
- Roche, A.E., et al., Validation of CH₄ and N₂O measurements by the cryogenic limb array etalon spectrometer instrument on the upper atmosphere research satellite, *Journal of Geophysical Research-Atmospheres*, 101 (D6), 9679-9710, 1996.
- Rotman, D.A., et al., Global Modeling Initiative assessment model: Model description, integration, and testing of the transport shell, *Journal of Geophysical Research-Atmospheres*, 106 (D2), 1669-1691, 2001.
- Schoeberl, M.R., A.R. Douglass, Z.X. Zhu, and S. Pawson, A comparison of the lower stratospheric age spectra derived from a general circulation model and two data

- assimilation systems, *Journal of Geophysical Research-Atmospheres*, 108 (D3), 4113, doi:10.1029/2002JD002652, 2003.
- Schubert, S.D., R.B. Rood, and J. Pfaendtner, An Assimilated Dataset for Earth-Science Applications, *Bulletin of the American Meteorological Society*, 74 (12), 2331-2342, 1993.
- Shindell, D.T., D. Rind, and P. Lonergan, Increased polar stratospheric ozone losses and delayed eventual recovery owing to increasing greenhouse-gas concentrations, *Nature*, 392 (6676), 589-592, 1998.
- Solomon, S., Stratospheric ozone depletion: A review of concepts and history, *Reviews of Geophysics*, 37 (3), 275-316, 1999.
- Strahan, S.E., and A.R. Douglass, Evaluating the credibility of transport processes in simulations of ozone recovery using the Global Modeling Initiative three-dimensional model, *Journal of Geophysical Research-Atmospheres*, 109 (D05110), doi:10.1029/2003JD004238, 2004.
- Waugh, D.W., D.B. Considine, and E.L. Fleming, Is upper stratospheric chlorine decreasing as expected?, *Geophysical Research Letters*, 28 (7), 1187-1190, 2001.
- Waugh, D.W., and T.M. Hall, Age of stratospheric air: Theory, observations, and models, *Reviews of Geophysics*, 40 (4), 1010, doi:10.1029/2000RG000101, 2002.
- Weaver, C.J., A.R. Douglass, and R.B. Rood, Thermodynamic Balance of 3-Dimensional Stratospheric Winds Derived from a Data Assimilation Procedure, *Journal of the Atmospheric Sciences*, 50 (17), 2987-2993, 1993.
- Woodbridge, E.L., et al., Estimates of Total Organic and Inorganic Chlorine in the Lower Stratosphere from in-Situ and Flask Measurements During Aase-II, *Journal of Geophysical Research-Atmospheres*, 100 (D2), 3057-3064, 1995.

Wu, J., and A.E. Dessler, Comparisons between measurements and models of Antarctic ozone loss, *Journal of Geophysical Research-Atmospheres*, 106 (D3), 3195-3201, 2001.

Figure Captions

Figure 1: Mean age of air in the GMI CTM as a function of latitude and pressure. Top left - mean age using FVGCM meteorological data. Top right - mean age using FVDAS meteorological data. Bottom left - mean age difference, FVGCM – FVDAS. Bottom right: Meridional dependence at 56 hPa of mean age in the FVGCM (solid line) and FVDAS (dashed line) simulations, compared with mean age estimates made using aircraft CO₂ observations (asterisks show the mean age from observations, and diamonds show the uncertainty range).

Figure 2: Observed and simulated N₂O on the: a. 650 K and b. 450 K potential temperature surfaces as a function of equivalent latitude. Solid blue line – N₂O from GMI_GCM simulation, averaged over the September 1 – September 18 time period. Solid red line - N₂O from GMI_DAS simulation, averaged over the September 1 – September 18 time period. Magenta asterisks with error bars: equivalent-latitude averaged N₂O from the CLAES instrument, averaged from September 1 to September 18. Error bars show ± 1 standard deviation of all observed values constituting the average. Green diamonds – equivalent latitude averages of ALIAS N₂O observations made during September, 1987 as part of the AAOE. Black diamonds – equivalent latitude averages of ALIAS N₂O observations made during October, 1994 as part of ASHOE.

Figure 3: Cold pool areas in the GMI_GCM and GMI_DAS simulations. a. Cold pool area in the GMI_GCM simulation as a function of day of year and potential temperature. The area below 195 K in the extratropical southern hemisphere is expressed as a percentage of the total surface area of the Earth. b. Same as in a, but for the GMI_DAS simulation. c. Difference in area

between the GMI_DAS and GMI_GCM simulations. A positive number means a larger pool in the GMI_DAS simulation and hence, a larger region of temperatures below 195 K.

Figure 4: Change in Antarctic ozone (ozone averaged over equivalent latitudes poleward of 65°S) between 1995 and 2030 as a function of day of year and potential temperature, in mixing ratio units. a. Difference between Antarctic ozone in 2030 and 1995 in the GMI_GCM simulation. b. Difference between Antarctic ozone in 2030 and 1995 in the GMI_DAS simulation.

Figure 5: Change in Antarctic ozone (ozone averaged over equivalent latitudes poleward of 65°S) between 1995 and 2030 as a function of day of year and potential temperature, in percent. a. Difference between Antarctic ozone in 2030 and 1995 in the GMI_GCM simulation. b. Difference between Antarctic ozone in 2030 and 1995 in the GMI_DAS simulation.

Figure 6: Antarctic ozone mixing ratio in parts per million by volume as a function of day of year during 1995 at a. 450 K, b. 550 K, and c. 650 K in the GMI_GCM (solid line) and GMI_DAS simulations (dashed line) simulations. Also shown are averages of observed ozone values for equivalent latitudes poleward of 65°S on each potential temperature surface from the MLS instrument in 1992 (red crosses), 1993 (blue crosses), and 1994 (green crosses), and the CLAES instrument (magenta crosses).

Figure 7: Antarctic ozone loss in the a. GMI_GCM and b. GMI_DAS simulations for 1995 at 450 K. Ozone loss is defined as the change in ozone since July 1. Solid line: simulated ozone

loss. Dashed line: integrated chemical ozone loss (see text for explanation). Dash-dot line: simulated loss minus integrated chemical loss, which can be interpreted as the effects of transport. Red, blue, and green crosses: vortex averaged ozone loss calculated from 1992, 1993, and 1994 MLS observations, respectively.

Figure 8: a. Time series of Antarctic Cl_y (solid lines) and Cl_x (dashed lines) in the GMI_GCM and GMI_DAS simulations during 1995 on the 450 K potential temperature surface. Cl_x is defined as $\text{ClO} + 2 \cdot \text{Cl}_2\text{O}_2$. Blue lines show GMI_GCM results and red lines show GMI_DAS results. Crosses are observationally-based estimates of Antarctic Cl_y from CLAES N_2O observations as discussed in text. b. Ratio of Antarctic Cl_x to Cl_y in the two simulations, as a percentage of Cl_y .

Figure 9: Equivalent-latitude averaged Cl_y comparisons. Magenta asterisks with error bars indicate Cl_y inferred from CLAES N_2O observations from September, 1992. Black crosses show Cl_y inferred from ATLAS N_2O observations made on NASA ER-2 flights in October, 1994, as part of the ASHOE mission. Green crosses - Cl_y inferred from ATLAS N_2O observations made on NASA ER-2 flights in September, 1987, as part of the AAOE mission.

Figure 10: Comparison of ozone loss at 450 K in 1995, 2030, and their difference. a. Shows ozone loss after July 1 during 1995 in GMI_GCM (solid blue line) and GMI_DAS (solid red line) simulations. Dashed blue and red lines are the corresponding losses for the year 2030. Dashed-dot lines show 2030-1995 difference for GMI_GCM (blue) and GMI_DAS (red). b. Shows chemically integrated ozone loss after July 1 during 1995 (solid lines), 2030 (dashed

lines) and the 2030-1995 difference (dashed-dot lines), for GMI_GCM (blue) and GMI_DAS (red). c. Shows net effect of transport after July 1 during 1995 (solid lines), 2030 (dashed lines) and the 2030-1995 difference (dashed-dot lines), for GMI_GCM (blue) and GMI_DAS (red).

Figure 11: Change in Antarctic Cl_y and Cl_x between 1995 and 2030 at 450 K in the GMI_GCM and GMI_DAS simulations. Solid blue (red) line corresponds to 1995 – 2030 change in time series of Cl_y averaged at equivalent latitudes above 65°S in the GMI_GCM (GMI_DAS) simulation. Dashed blue (red) line corresponds to 1995 – 2030 change in time series of Cl_x averaged at equivalent latitudes above 65°S in the GMI_GCM (GMI_DAS) simulation.

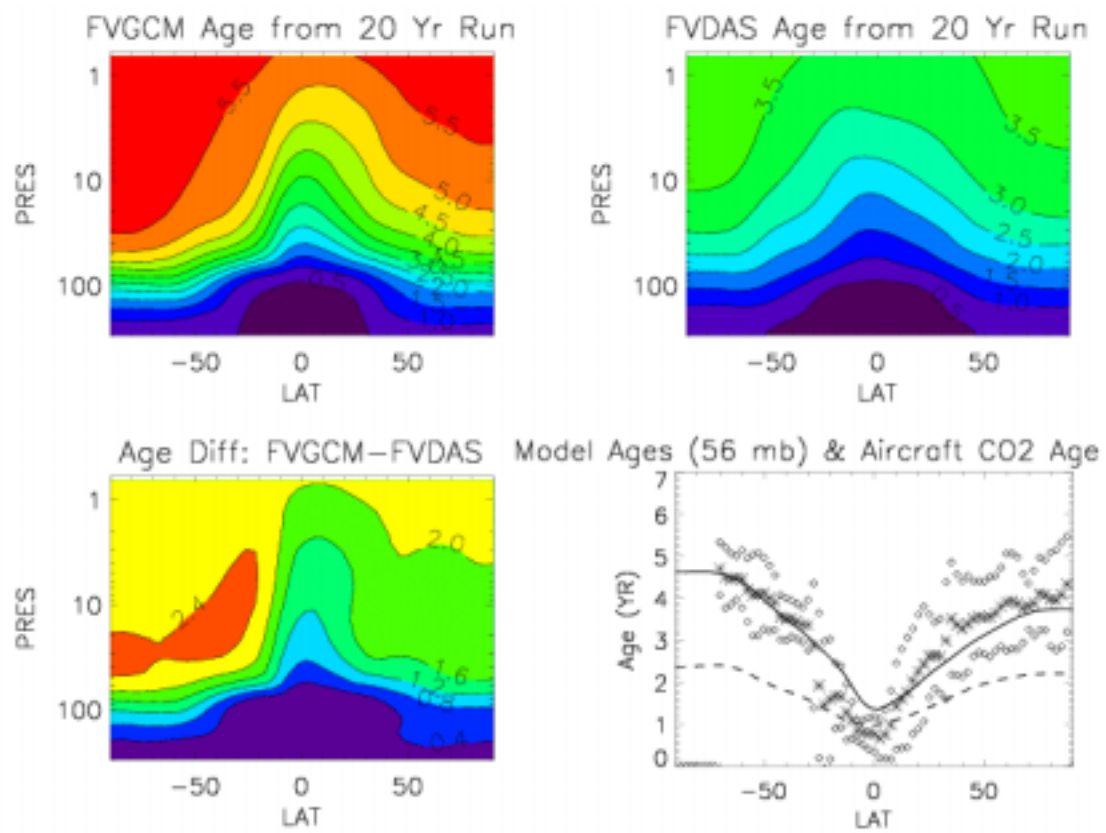


Figure 1

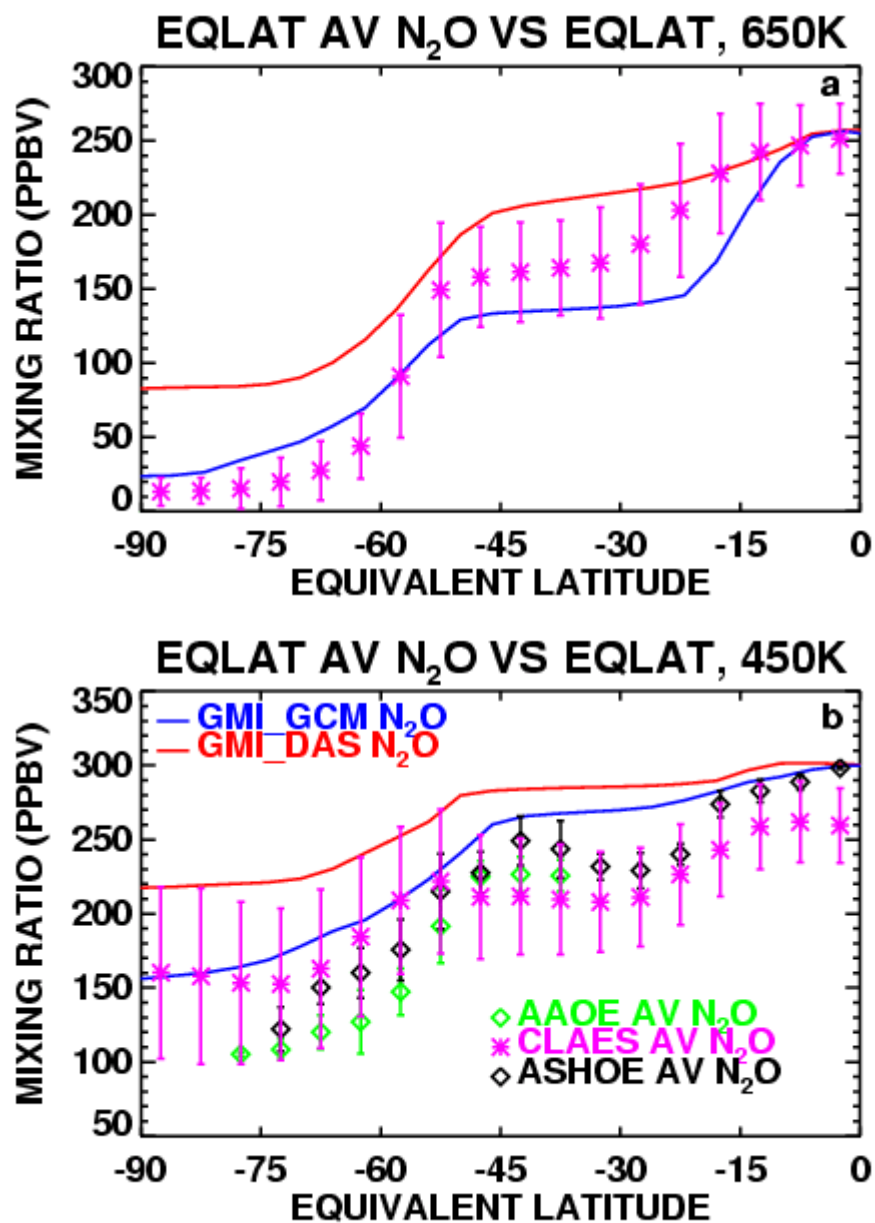


Figure 2

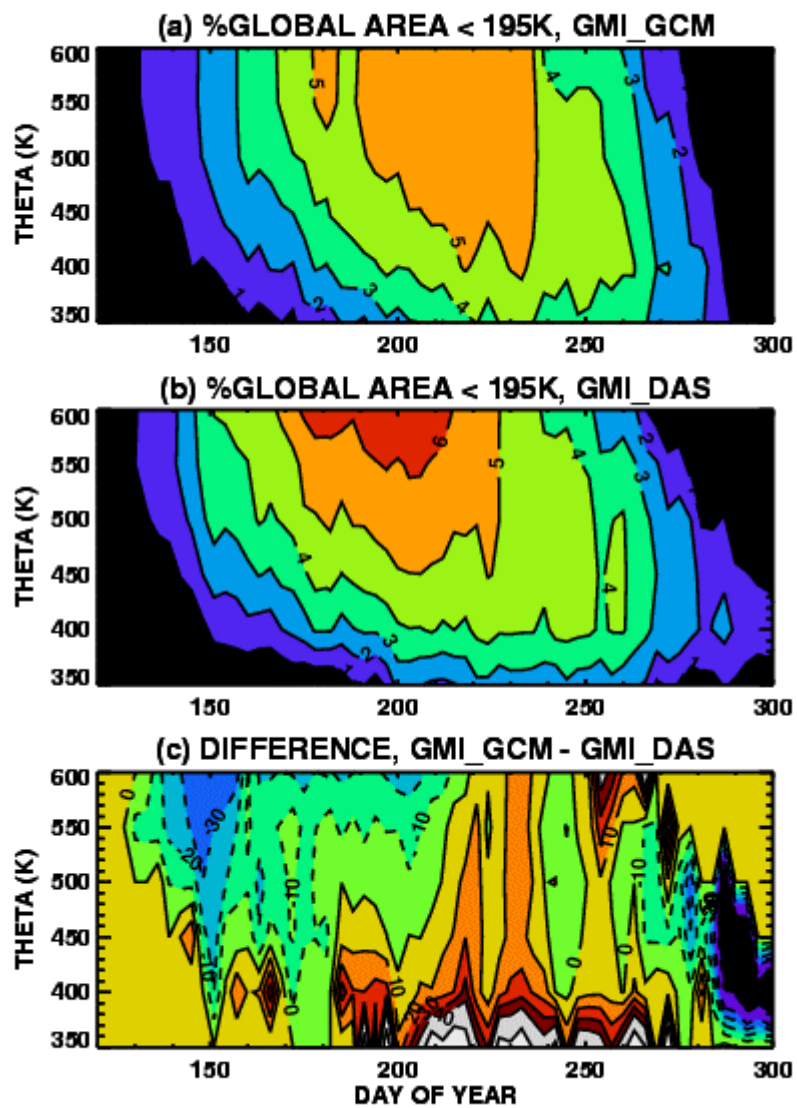


Figure 3

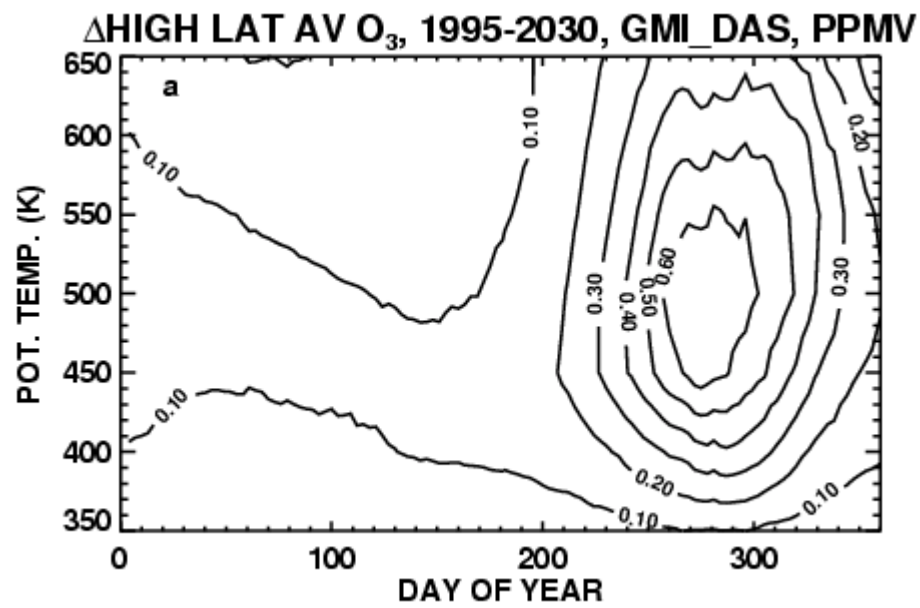
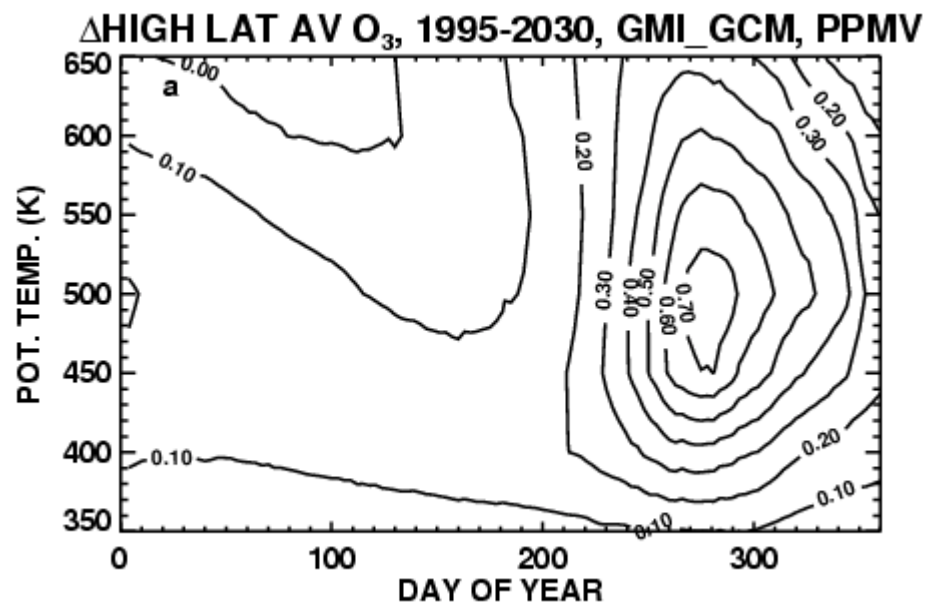


Figure 4

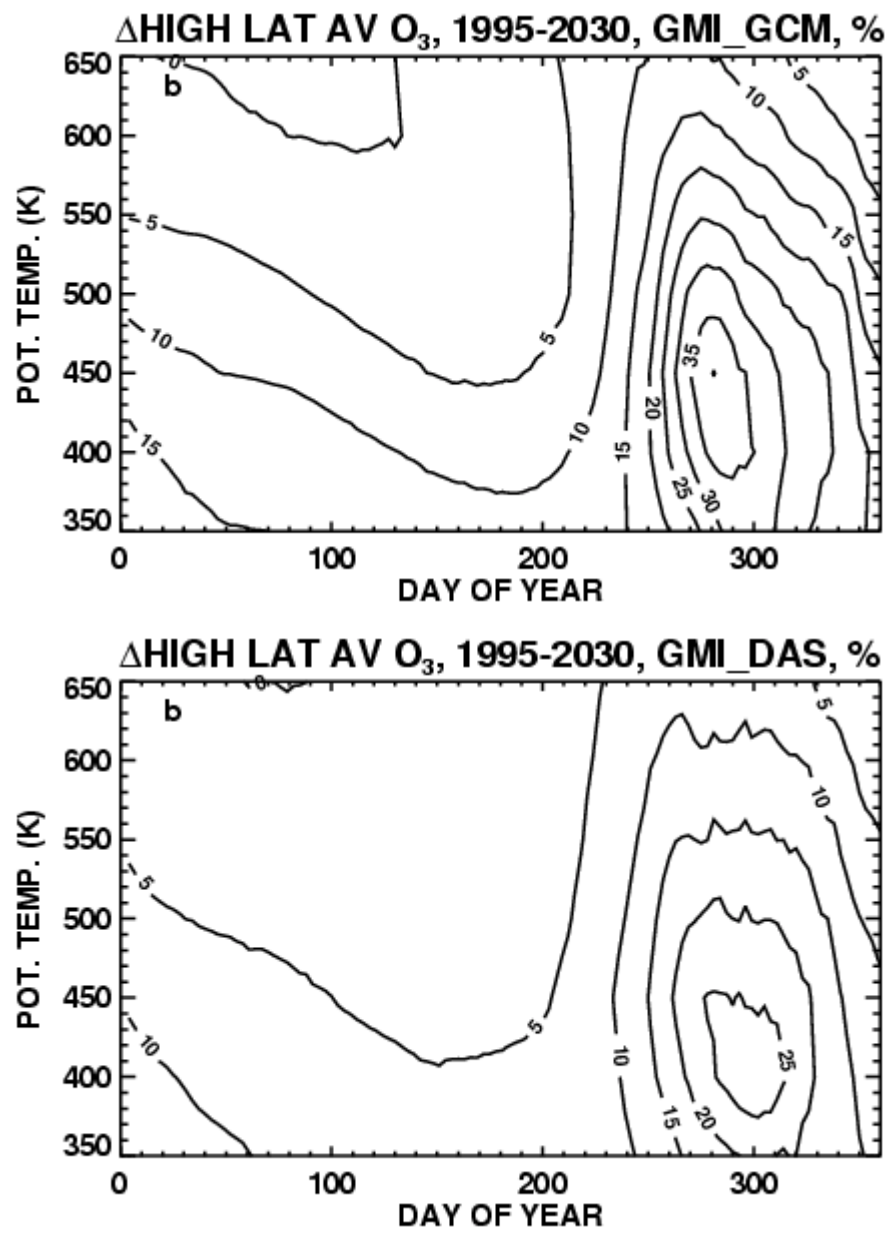


Figure 5

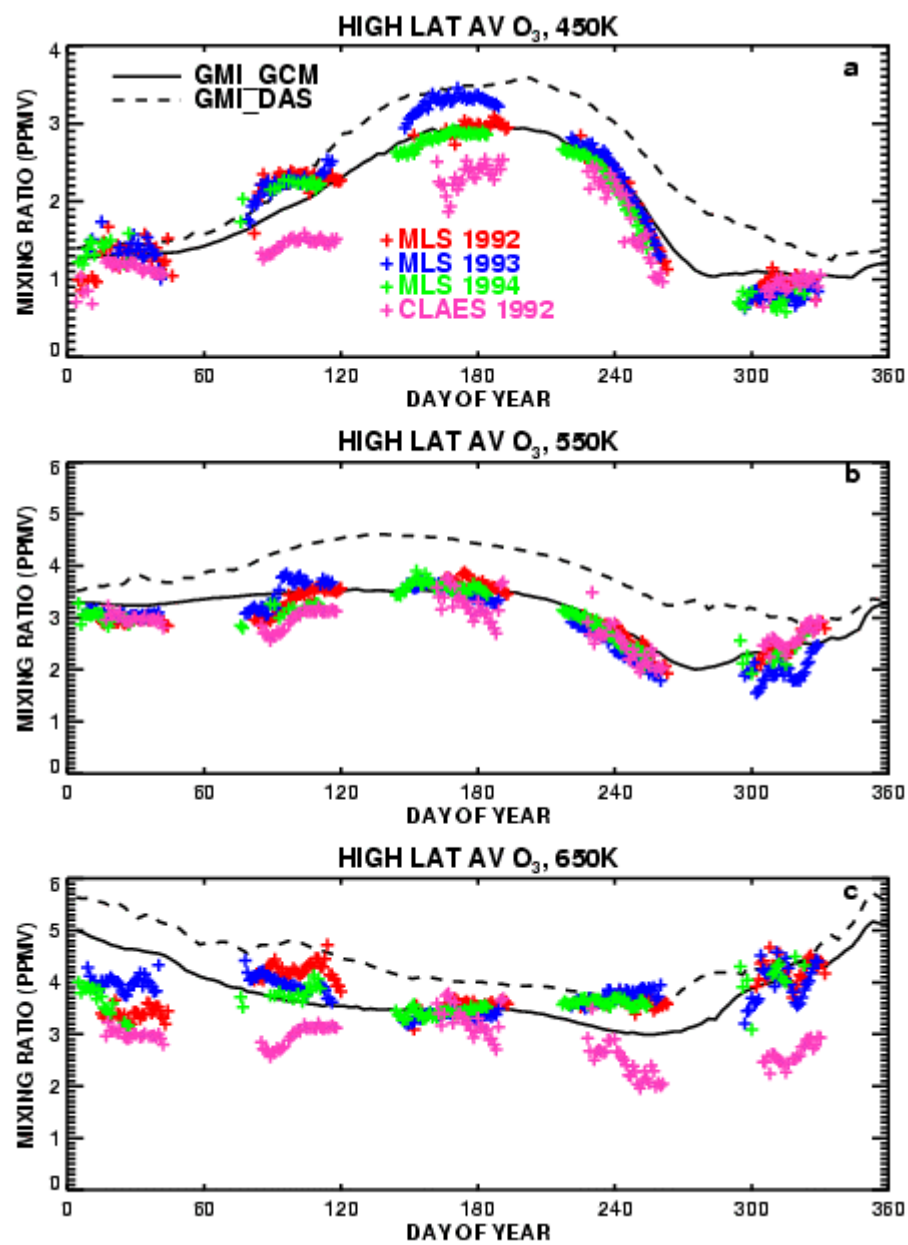


Figure 6

HIGH LAT AV O₃ LOSS, 450K, GMI_GCM

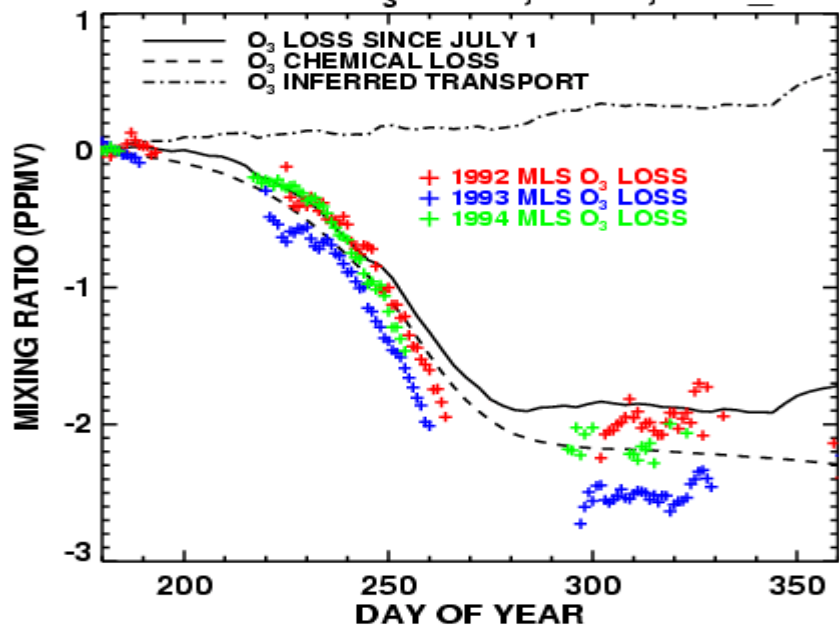


Figure 7a

HIGH LAT AV O₃ LOSS, 450K, GMI_DAS

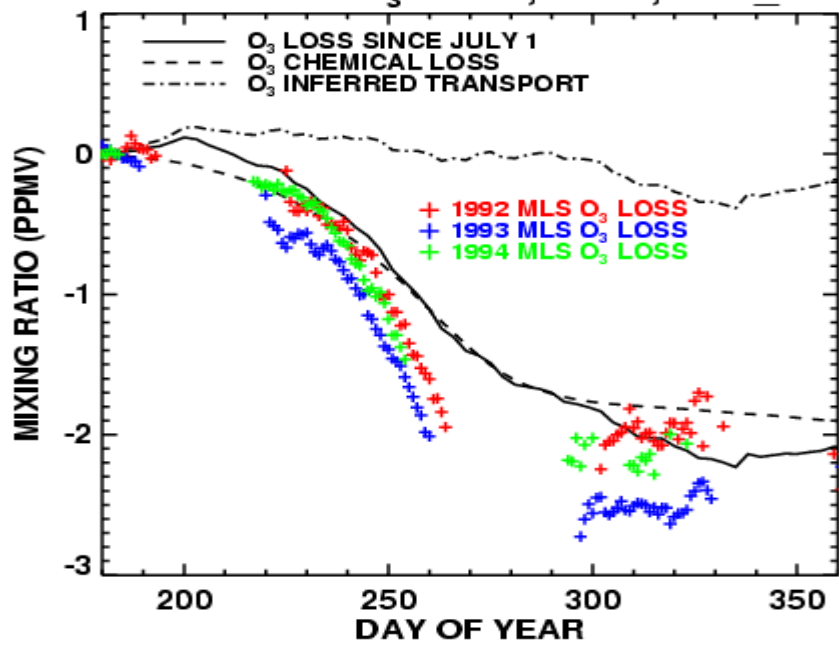


Figure 7b

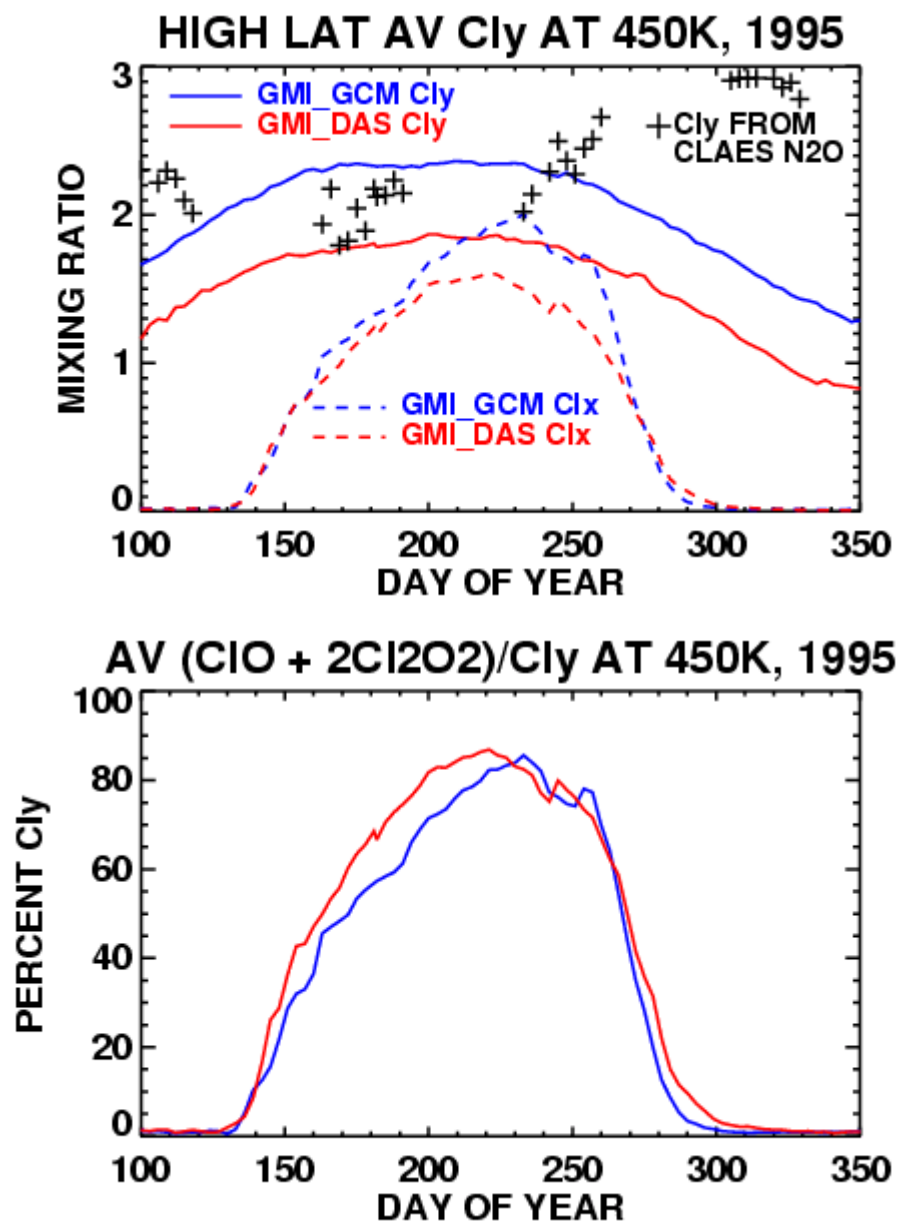


Figure 8

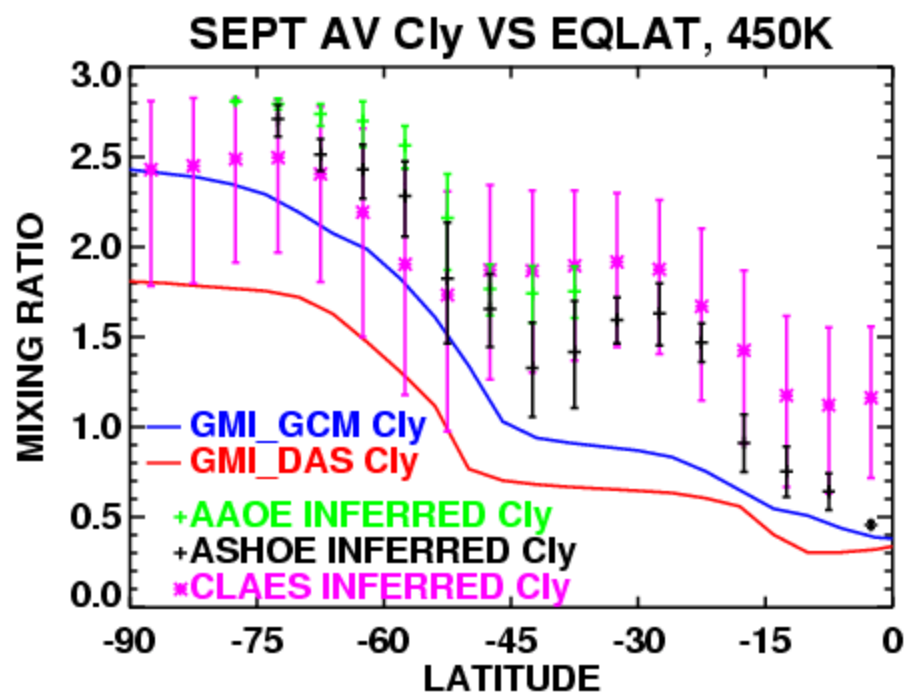


Figure 9

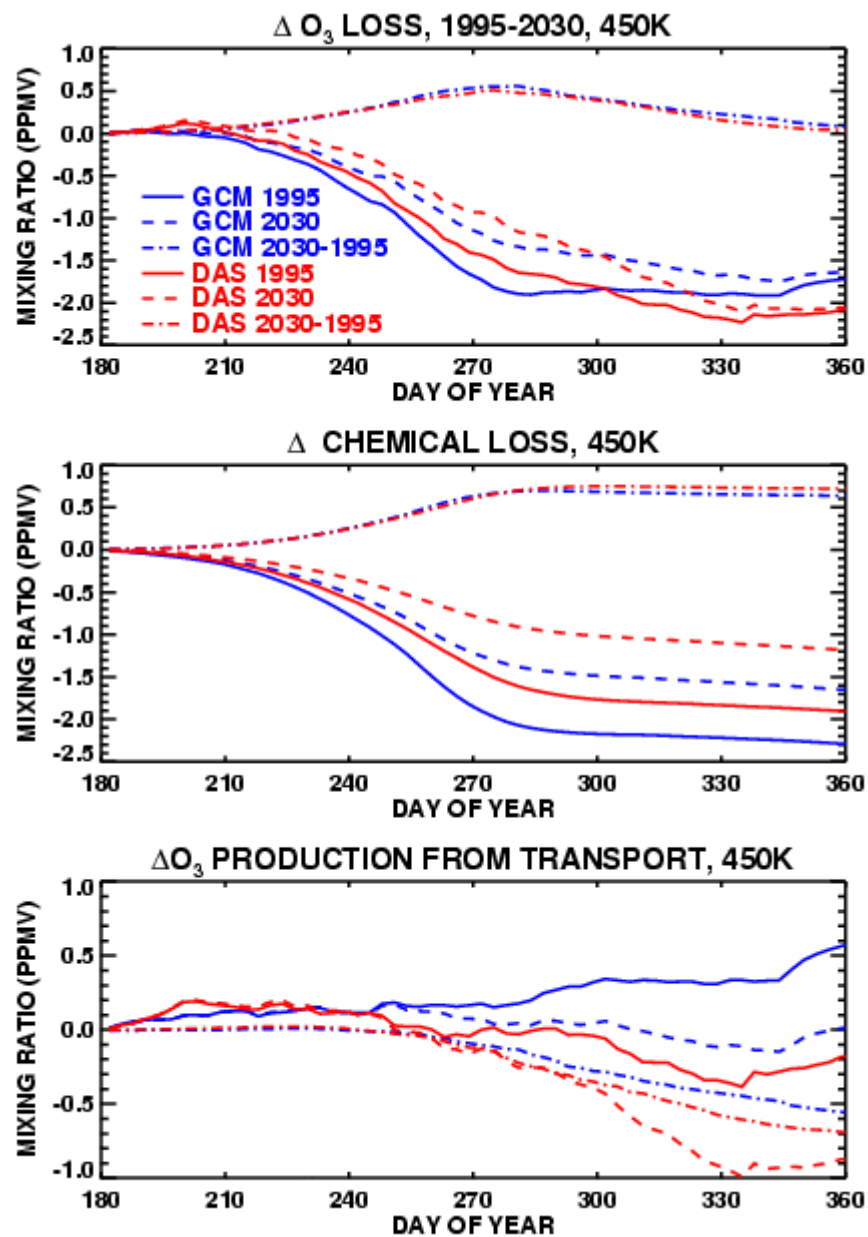


Figure 10

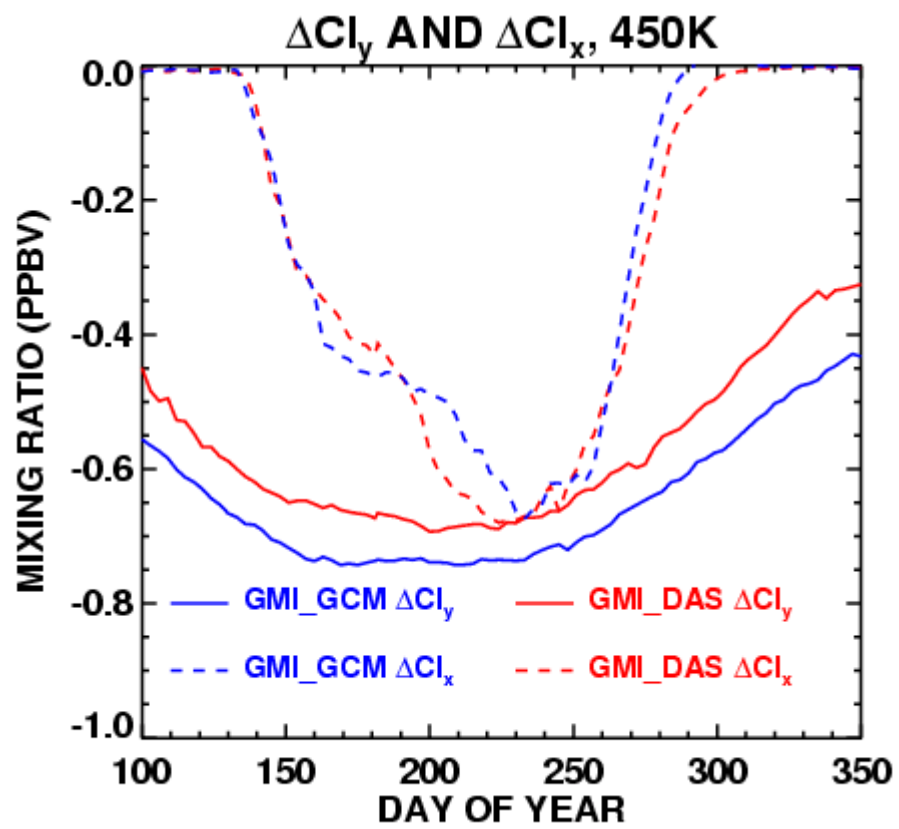


Figure 11